
Article:
Ryvkin, B. S., Avrutin, E. A. orcid.org/0000-0001-5488-3222, Kostamovaara, J. E K et al. (1 more author) (2017) Laser diode structures with a saturable absorber for high-energy picosecond optical pulse generation by combined gain-and Q-switching. Semiconductor science and technology. 025015. ISSN: 0268-1242

https://doi.org/10.1088/1361-6641/32/2/025015

Laser diode structures with a saturable absorber for high-energy picosecond optical pulse generation by combined gain-and Q-switching.

B.S.Ryvkin [1,2] , E.A. Avrutin [3], J.E.K. Kostamovaara[1], J.T.Kostamovaara[1],

[1] Dept of Electrical and Information Engineering, University of Oulu, Oulu, Finland

[2] A.F.Ioffe Physico-Technical Institute, St.Petersburg, Russia

[3] Dept of Electronics, University of York, York, UK

Abstract:

The performance of gain-switched Fabry-Perot asymmetric-waveguide semiconductor lasers with a large equivalent spot size and an intracavity saturable absorber was investigated experimentally and theoretically. The laser with a short (~ 20 μm) absorber emitted high-energy afterpulse-free optical pulses in a broad range of injection current pulse amplitudes; optical pulses with a peak power of about 35 W and a duration of about 80 ps at half maximum were achieved with a current pulse with an amplitude of just 8 A and a duration of 1.5 ns. Good quality pulsations were observed in a broad range of elevated temperatures. The introduction of a substantially longer absorber section lead to strong spectral broadening of the output without a significant improvement to pulse energy and peak power.

Introduction: Picosecond-range (~100 ps) high energy optical pulse generation with semiconductor lasers has attracted significant attention recently, with a view for obtaining compact optical sources for applications such as high-precision laser radars (the most immediate intended application in our studies) three-dimensional (3-D) time imaging, spectroscopy and lifetime studies. Pulses of such duration, or shorter, have been reported by a large number of authors since the early days of laser diode technology (see e.g. [1,2] for an overview). The main techniques used are gain switching (pumping the laser with a current pulse of a nanosecond duration or somewhat shorter, but still significantly longer than the desired optical pulse), active or passive Q-switching (using a laser incorporating an active voltage-controlled modulator or a saturable absorber respectively), or a combination of these techniques. The general principles of all these regimes have been relatively well understood

for some time, however achieving the performance required in a practical system is not trivial. The two main, and somewhat conflicting, requirements need to be satisfied. Firstly, a high pulse energy (significantly above 1 nJ) needs to be achieved in a pulse about 100 ps long (a shorter pulse is not necessary in a laser radar system using Single Photon Avalanche Photodetectors, since 100 ps is the typical timing jitter of those photodetectors, see e.g. [3]). Secondly, pulses generated needs to be free, or nearly free, from any afterpulsing structure. In addition to these essential requirements, operation in a single transverse (and ideally lateral) mode is beneficial, as is compatibility with a silicon pumping pulse source generating pumping pulses with an amplitude of about 10 A. Finally, a narrow to moderate spectral linewidth is also highly desirable for many applications.

We have proposed [4,5] and experimentally realised [6-8] an asymmetric waveguide gain-switched laser design, involving the refractive index contrast at the interface between the Optical Confinement Layer (OCL) and the *p*-cladding substantially greater than that at the interface between the OCL and the *n*-cladding, and the active layer position shifted from the peak of the transverse mode towards the *p*-cladding. Such a structure has the advantage of supporting strictly one transverse mode, with a large equivalent spot size $d_a/\Gamma_a >> 1$ (d_a and Γ_a being the active layer thickness and the confinement factor, respectively). As shown in [4,5,9], the large d_a/Γ_a allows for a large number of carriers to be accumulated before the onset of the optical pulse (hence high pulse energy), while positioning the high-energy optical pulse at the trailing edge of the pumping pulse, facilitating afterpulsing-free operation in a broad range of currents. Both bulk [6-7] and Quantum Well [8] active layers where realised, with good performance. Compared with other laser designs realising a very large d_a/Γ_a, such as the Slab Coupled Optical Waveguide Lasers (see e.g. [10]), the asymmetric waveguide design has the advantage of allowing single transverse mode operation in a broad stripe laser (albeit at the cost of laterally multimode emission), and thus higher total pulse energies and peak powers.

The introduction of a short (20-30 μm long), unbiased saturable absorber section next to the antireflection facet of the (bulk active layer) asymmetric waveguide laser allowed the range of afterpulsing-free operation to be extended further, up to 35 W in terms of peak pulse power, or 3.5-4 nJ of pulse energy [7]. Apart from removing the afterpulses, this simple short absorber did not have a substantial effect on the (main) pulse shape, amplitude, and energy.

There have been previous reports [11-14] of combining gain-switching and passive Q-switching in high-power lasers, in which the introduction of a saturable absorber allowed the picosecond pulse energy to be substantially increased compared to purely gain-switched operation. Both bulk and Quantum Well active layer lasers can be used in principle. In [12], a Single Heterostructure laser was used, with very high pulse power and energy (~380 W peak power in a 40 ps long pulse) achieved, but with multiple transverse mode operation and at very high injection currents (~40A). The saturable absorber in [12] was implemented by ion implantation of a part of the laser cavity.

Here, we investigate the effects of a simplest Saturable Absorber (SA), in the form of an unbiased waveguide section, on the performance of an (intrinsically single-mode) asymmetric-waveguide bulk double heterostructure laser with a large d_a/Γ_a . Optical pulses with a peak power of about 35 W (similar to that obtained in [7]) and a duration of about 80 ps at half maximum were achieved with a 1.5 ns long current pulse with an amplitude of just 8 A (about half of that used in [7]).

2.1. A saturable absorber in a monolithic diode laser: general considerations.

Absorption saturation in semiconductors under high-power light incidence happens, most straightforwardly, due to band filling (dynamic Moss-Burstein) effect which is also affected by the screening of Coulomb interaction between carriers (see e.g. [15] and references therein for bulk materials, [16] for Quantum Wells). In edge-emitting laser diode structures intended for fast pulse generation, the saturable absorber is implemented as an unpumped section of the laser waveguide, electrically isolated from the main part of the laser – the forward biased gain section. In most designs, the absorber is reverse biased. This is done, first and foremost, to speed up the absorber recovery due to the carrier sweepout by the electric field, which is important for high rate operation. However the external bias also affects the physics of absorption saturation which in the presence of bias is (in addition to band filling effect which decreases with increased electric field values) affected by the interplay of the electroabsorption (Franz-Keldysh effect in bulk materials and Quantum Confined Stark effect in nanostructures) and voltage redistribution between the SA and the external or internal resistance (see e.g. [16,17,18]). In combined gain/Q-switching, when very high repetition rate are not required, it is not essential to have fast absorption recovery. Then, it would appear that the external bias on the absorber is not required, which leaves the band filling as

the sole absorption saturation mechanism and substantially simplifies the laser design and handling. However, as has been convincingly shown in a recent experimental paper [14], in the case of a Quantum Well laser structure, an unbiased or weakly biased absorber does not allow high power/high energy pulse generation to be achieved under combined gain/Q-switching operation. The reason is that in this case, the operating wavelength of a Quantum Well laser (which is affected by the bandgap shrinkage in the gain section) is at the long-wavelenth tail of the SA absorption spectrum, meaning that the unsaturated absorption is low, and the saturation (Q switching) does not significantly affect the gain-switching pulse parameters. The situation is however quite different in bulk active layer laser structures. In this case, the bandgap shrinkage is largely balanced by the short-wavelength shift of the gain peak with increased carrier density. Then, even without the external bias, the operating wavelength corresponds to a photon energy above the fundamental absorption edge, meaning that substantial saturable absoption is introduced, and deep nonlinear modulation of the cavity Q factor is possible, without applying any bias to the absorber. The possibility of using a laser without a separate contact to the absorber section is rather useful for devices intended for mass applications, where a simple design is a significant advantage [7], [19]. The ion implantation technique used in [12-13] gives very short absorber recovery and thus is not the ideal technology for applications requiring high pulse power and energy rather than high operation frequency or very short pulse duration at relatively low injection current values.

Therefore in the current paper we shall analyse lasers with bulk active layers and saturable absorbers in the form of an unbiased longitudinal section of the laser resonator, otherwise identical to the gain section. The paper continues the investigations started in [7] and presents more systematic studies on the effect of the absorber fraction (including values greater than those used in [7]) and the temperature performance.

2.2 Experimental.

The lasers studied were fabricated from a structure similar to that used in [7], grown by Innolume GmbH, Dortmund, Germany, with a higher quantum efficiency of 0.7-0.75 which results in a decrease in the injection current required. The structure used a Broad Asymmetric Waveguide design in the sense discussed in [20] (i.e. an asymmetric waveguide

with most of the transverse mode power localised in the OCL rather than the claddings). Similar structures have been shown to be well suitable for gain switching applications [4,7,21] and also promising for steady state high power lasing (see e.g. [20, 22-24]).
The structure used here has a bulk active layer (of a thickness d= 800 Å) shifted towards the p-cladding so as to give the equivalent spot size d/Γ_a >>1, Γ_a being the optical confinement factor (d/Γ_a≈2.7 μm in this case). Broad area lasers with a stripe width of 90 μm and a cavity length of 1.5 mm were investigated; the facets were coated to provide the low and high reflectances of approximately 0.05 and 0.95 respectively. As in [7], a fraction of the laser cavity length was left unpumped, forming the simplest saturable absorber.

In the following experiments, the laser diodes were driven with a custom pulse generator that consist of a MOS switch and an LCR transient circuit [27,28]. In this kind of a driver, the current pulse amplitude and width are determined by the supply voltage (in the range of ~100V) and the √LC time constant of the circuit, respectively. A current amplitude and a pulse width of ~10A and 1-1.5ns, respectively, can be quite straight-forwardly produced at a pulsing rate of ~100kHz. The optical pulse shapes were measured with a high-speed optoelectronic converter (1414 New Focus, 25GHz) and a high speed real-time oscilloscope (Agilent DS091204A, 12GHz). The output of the laser diode under measurement was carried with a short optical fibre (with the core diameter of 50 μm, so the emission from the entire stripe was effectively captured) to the OE converter.
The results given are based on averaging many successive pulses from the oscilloscope which should somewhat improve the temporal precision, but otherwise are given as they were recorded without any corrections with regard to the bandwidth of the measurement system. Therefore the pulse amplitudes and durations may still be affected by the measurement resolution. We note however that for LIDAR applications, it is the pulse energy (proportional to the number of photons in the pulse) that is the more important parameter, and that can be expected to not be affected by the system resolution.

Figure 1 shows the measured time profile of optical pulses alongside the corresponding electrical pumping pulses, whose amplitude was varied in a moderately narrow range (≈ 9-12 A), for the case of the saturable absorber length of 20 (a) and 100 (b) μm. The pumping pulse duration and shape were kept approximately constant, and the measurements were conducted at room temperature. Qualitatively, the behaviour of the optical pulses is similar to that

measured in [7]: the optical pulse emerges at a certain pulse amplitude (the dynamic threshold) at the trailing edge of the pumping pulse; then, as the pumping pulse amplitude is increased, the optical pulse moves forward in time, increases in amplitude and gradually acquires an afterpulsing structure which approximately follows the pumping pulse profile. Comparing the parameters of the emitted pulses at similar pumping pulse amplitudes with different absorber lengths, we note that, as can be expected, the dynamic threshold of a laser with a longer SA is higher, and the laser switches on more sharply than the one with the shorter SA. However, there is a broad range of current amplitudes within which the values of the peak power (and energy) of the optical pulse for both absorber lengths are very similar; note that both designs allow a peak power of about 40 W with a very small trailing structure to be achieved with a current amplitude of about 10 A, with the trailing structure for the 100 µm SA laser being somewhat smaller.

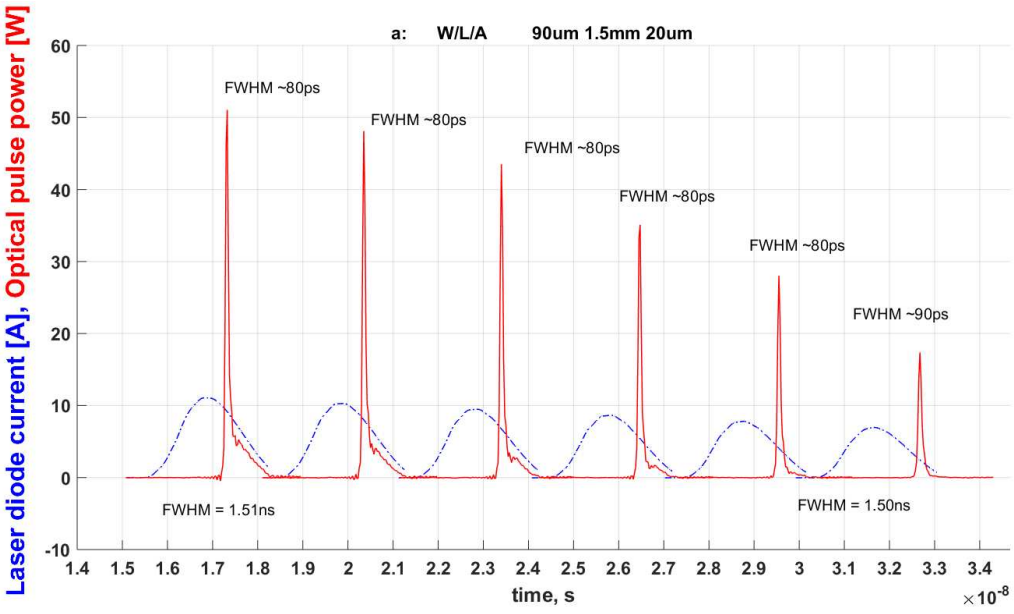

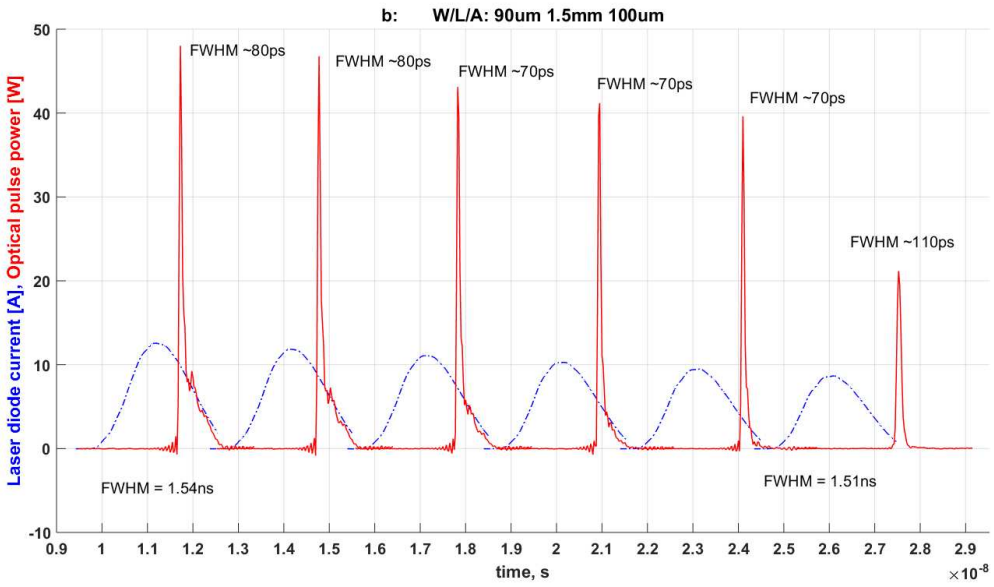

Figure 1. The optical output of the laser diode (stripe width 90um, cavity length 1.5mm) as a function of the pulse current. a) saturable absorber length 20um, b) saturable absorber length 100um. Note, that the separate results are shown in a single figure to enable one to compare the results easier, and the pulse durations indicated are approximate values partly determined by the measurement resolution.

There is however a much more significant difference in the *spectra* of the laser emission (Figure 2) depending on the length of the SA, with the spectrum for the case of a longer absorber being about twice wider than that of a laser with a shorter absorber for the same current. Qualitatively, this can be explained by a wider variation in the carrier density during the pulse in the case of a longer absorber, combined with a strong shift of the spectral gain peak with carrier density in the bulk active layers used here; see also the calculation results below.

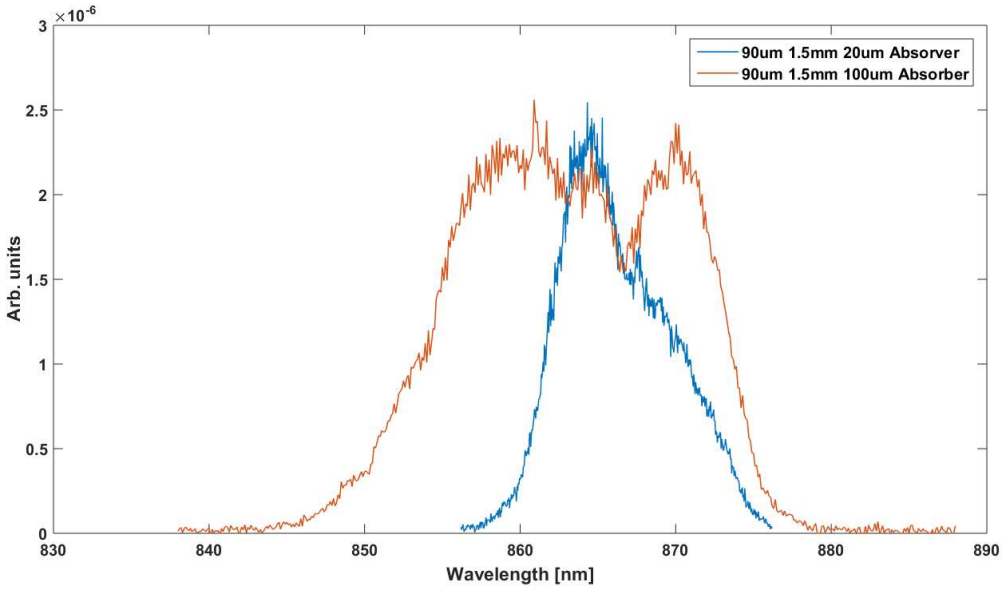

Figure 2. Optical output spectra of the laser diodes (stripe width 90um, cavity length 1.5mm) with the saturable absorber lengths of 20um and 100um. Drive current pulse amplitude and width ~10A and ~1.5ns, respectively.

For range finding, which is the main targeted application for these lasers, the narrower spectrum is strongly preferred [29], given the similar pulse power and energy, since the narrower laser spectrum makes it easier to filter out background radiation at detection. Therefore, below, we shall mainly concentrate on lasers with the shorter SA.

The intended application also makes it important to analyse the temperature performance of the lasers, since in a real range finding device they will be located next to a driver and see substantial current heating, in addition to being operated in a broad range of ambient temperatures. Figure 3 shows the pulse profiles of the laser with a SA 20 μm long measured at the same driving pulse amplitude (11 A) and various operating temperatures. In a broad range of temperatures (from about 0 C to 55C) the peak pulse and energy are relatively weakly affected by temperature; unfortunately this corresponds to the situation when the optical pulse has a substantial afterpulsing structure. With further increase in temperatures, the decrease in optical gain (at a constant carrier density) with temperature leads to a significant increase in the static and dynamic threshold of the laser operation. Thus the optical pulse shifts towards the trailing edge of the pumping pulse, decreases in amplitude, and loses the afterpulsing structure. In other words, while detrimental for pulse energy, the temperature increase inherent under realistic operating conditions may have a beneficial effect as regards the pulse *shape*. It takes a temperature as high as about 80C for the

temperature induced decrease in pulse energy to become too significant for the intended applications.

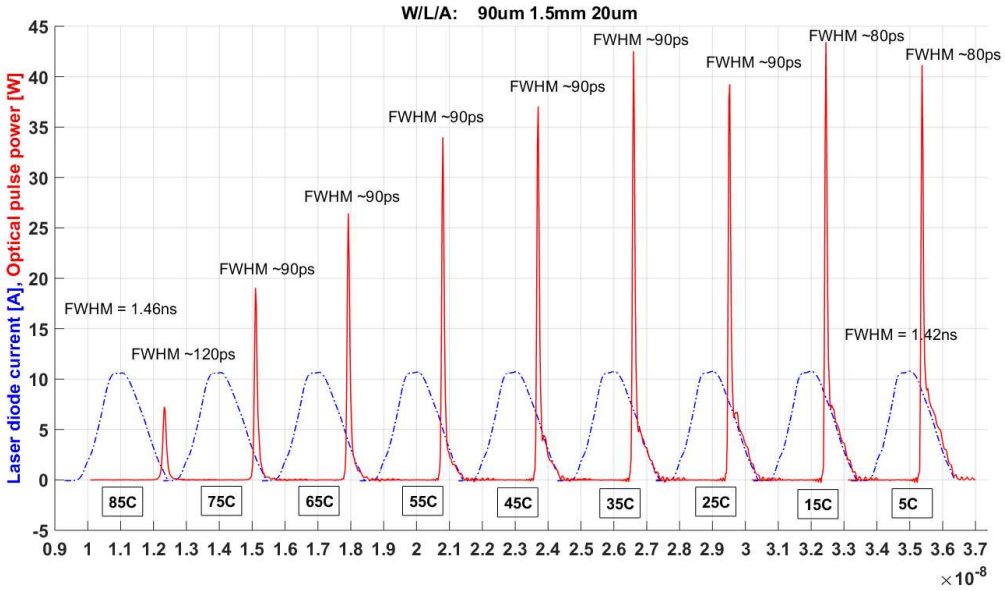

Figure 3. Optical output of the laser diode with a cavity length, stripe width and saturable absorber length of 1.5mm, 90um and 20um, respectively, as a function of ambient temperature.

2.3. Calculations.

Most of the simulations were performed with the in-house Travelling Wave model LasTiDom, as described in previous papers (see e.g. [25]), though we note that for most cases (except the longest absorber lengths and very large unsaturated absorption) most of the results (except the lasing spectra) were reproduced fairly well by simple rate equation simulations.

The laser and pumping pulse parameters used are summarised in Table 1.

For the peak gain dependence on the carrier density in our bulk active layers, we used a simple semi-microscopic formula obtained in the early paper by R.F.Kazarinov [26]:

$$g(N,T) = g_{0p}\left[\frac{N}{N_v(T)} - \exp\left(-\frac{1}{4\pi}\left(\frac{3\pi^2 N}{N_c(T)}\right)^{2/3}\right)\right] \qquad (1)$$

, where N_c and N_v are the effective densities of states in the conduction and valence band respectively. With the coefficient g_0 set as 2700 cm^{-1}, the formula coincides remarkably well with the well-tested three-parameter logarithmic approximation given in [27] for gain in bulk

GaAs at T=300K. However, the use of the semi-microscopic formula gives us the option to include the temperature dependence of gain in future work, by using the temperature dependent N_c and N_v. As in previous papers [4,5], the gain spectrum was modelled using an infinite response digital filter, corresponding in frequency domain to a Lorentzian. The peak position and width were taken as carrier density dependent; specifically, the spectral shift of the gain peak frequency ω_{peak} with carrier density was taken as linear, in good agreement with microscopic calculations using a model similar to that of [28,15], from which the value of $d\omega_{peak}/dN=1.6\times10^{-5}$ $s^{-1}cm^3$ was taken; the broadening of the gain spectrum with carrier density was taken as approximately twice this value, so as to keep the long-wavelength edge of the gain spectrum approximately in the same place, also as suggested by microscopic calculations.

For the carrier density dependence of the absorption in the SA, we used the simple and often used linear dependence

$$\alpha(N)= \alpha_0-\sigma N \qquad (2)$$

There are two main reasons for the choice of the simple linear approximation. Firstly, in steady state, it leads to the well-known saturation law $\alpha(I)= \alpha_0(1+I/I_s)^{-1}$ of a slow saturable absorber, where I is the radiation fluence and I_s is the saturation fluence value. Secondly and most importantly, we found that, with the high power pulses we are simulating, the absorber is very quickly (typically within the first half of the leading edge of the pulse) saturated completely, which makes the precise form of the $\alpha(N)$ dependence not too important given a correct value of the unsaturated absorption α_0 and a roughly correct carrier density α_0/σ for full absorption saturation. Calculations using the model of [28,15] imply that with the bulk material used in the experiments, the operating wavelength is within the plateau of the absorption spectrum, therefore the width of the absorption peak was taken much larger than that of the gain peak.

As with the previous work [4,5], the model used in the calculations is one-dimensional (plus time), ignoring the laterally multimode structure of the light emission. Analysis of lateral effects is reserved for future work, but we note that, as in [7], at least the time-averaged intensity from the laterally multimode laser was reasonably homogeneous across the stripe width.

Figure 4 shows the calculated pulse profiles for the structure with a 20 µm long SA for different pumping pulse amplitudes at room temperature. As in [4]; the results from the travelling wave model have been smoothed to remove the fast oscillations because of multimode dynamics. For the highest value of current pulse amplitude (10 A), the unsmoothed curve and the pumpling pulse profile (taken to have the shape of a half-period of a raised cosine, with a FWHM of 1.5 ns) are also shown to illustrate the positions of the optical pulse on the pumping pulse profile.

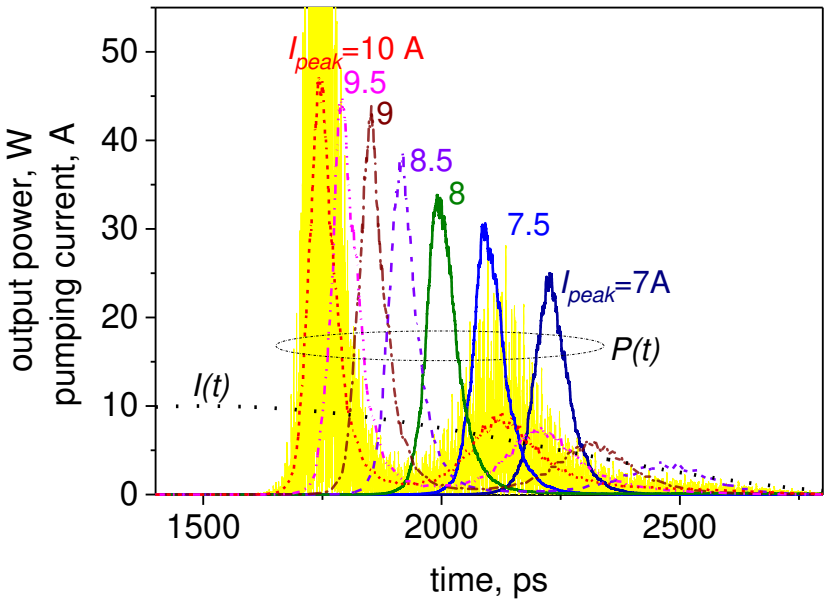

Figure 4. Calculated pulse shapes (filtered) as function of injection current amplitude. For I_{peak}=10 A, parts of an unfiltered profile (pale line) and current pulse are also shown.

Figure 5 compares the calculated and measured peak powers and energies.

We believe the theory reproduces most of the important features of the experimental results for the laser with a 20 µm SA length. The amplitudes and shapes of the main pulse are close to those observed experimentally, as is the current range for afterpulsing-free operation. The precise temporal structure of the afterpulsing, which in the experiment follows the pumping pulse profile almost adiabatically, is only reproduced well at high current amplitudes, both in the rate equation approach and the travelling wave model.

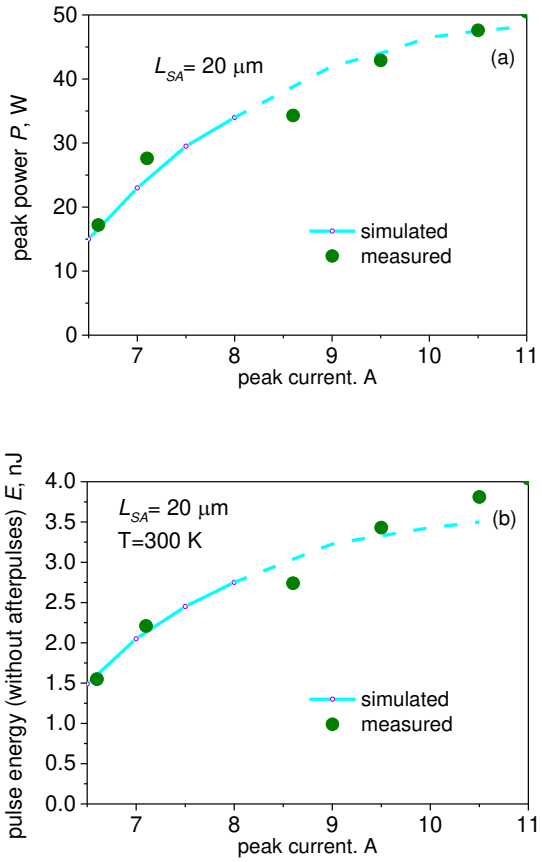

Figure 5. Comparison of measured (dots, as in Figure 1a) and simulated (line, solid-afterpulsing-free, dashed-with afterpulses) peak pulse power (a) and pulse energy (b).

For a laser with a longer saturable absorber (100 μm, so that $\alpha_0 L$>1), the agreement between the theory and measurements is less satisfactory. Most importantly, the theory predicts (in line with previous theoretical studies) that both the peak power and total energy of the optical pulse in a laser with a longer SA must be *higher* than in that with the shorter SA in a broad range of current pulse amplitudes. This is not the case in the experiment. While it can be argued that the disagreement in the peak optical power might be explained by the temporal resolution of the measurement system, this is not the case with the total pulse energy (which, as mentioned above, is the more important parameter for LIDAR applications). Therefore, it looks likely that some effective unsaturable absorption (weak enough to not matter in a short SA but significant in a longer one) is introduced in an unpumped laser section alongside the saturable absorption. The nature of this unsaturable absorption will be the subject of further study.

However, we note that there is a reason why a laser with a shorter absorber may be preferable to the longer absorber one, regardless of the pulse energy and peak power. Figure 6 shows the spectra of simulated optical pulses for the laser with the 20 μm long SA at different operating currents; for comparison, the spectra for the laser with the long (100 μm) SA are also shown. As in the experiment, the spectra of the 100 μm SA lasers are about twice wider than those of the 20 μm SA and broaden significantly with current, almost entirely towards the short-wavelength side of the spectrum (due to the higher carrier density value stored in a laser with a longer SA, hence the gain peak at the start of the pulse blue-shifted compared to the case of a laser with a shorter SA; in both cases the carrier density is depleted after the pulse to values close to transparency, hence a similar position of the gain peak after the pulse, determining the same long-wavelength edge of the spectrum). The numerical values of the total spectral widths are also closed to those measured experimentally. This confirms that the broad spectrum of the pulses with a long SA is indeed an inherent feature that follows from the broad carrier density variation, and reinforces our choice of the shorter SA design for further study.

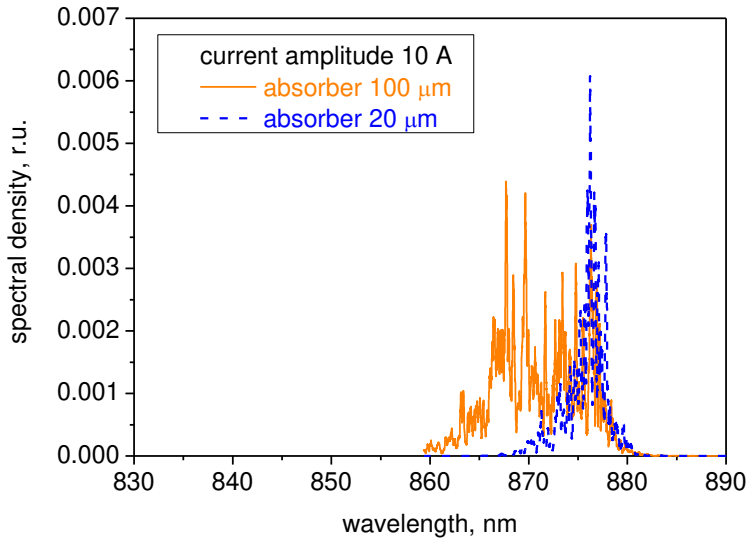

Figure 6. Simulated spectra of laser emission for two different saturable absorber lengths.

The good agreement between the experiment and calculations, for the shorter absorber case, allows us to use the model to estimate the laser performance for a different laser design. An example is shown in Figure 7, which shows that in increased equivalent spot size (d/Γ_a=4 μm) maintains afterpulsing-free operation at higher current values and thus allows an

afterpulsing free pulse with a somewhat higher peak power than what is available from the current laser to be achieved, if with somewhat higher pumping current pulse amplitude.

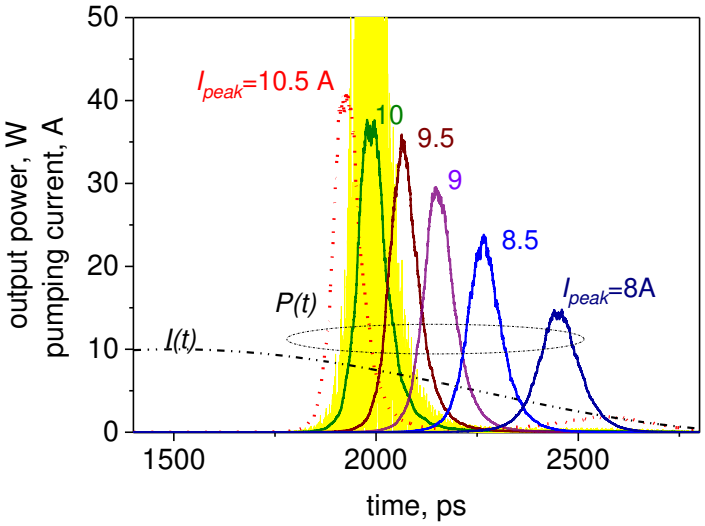

Figure 7. Predicted pulse shapes at different current pulse amplitudes for a laser with a larger d/Γ_a value of 4 μm.

Figure 8 compares the total energies of pulses generated by the laser with two values of d/Γ_a . As seen in the Figure, the potential advantage of a laser with a higher d/Γ_a is somewhat higher when measured in terms of pulse *energy* than pulse power. This of course means that the pulse is somewhat broader, but still within the specifications for the intended application.

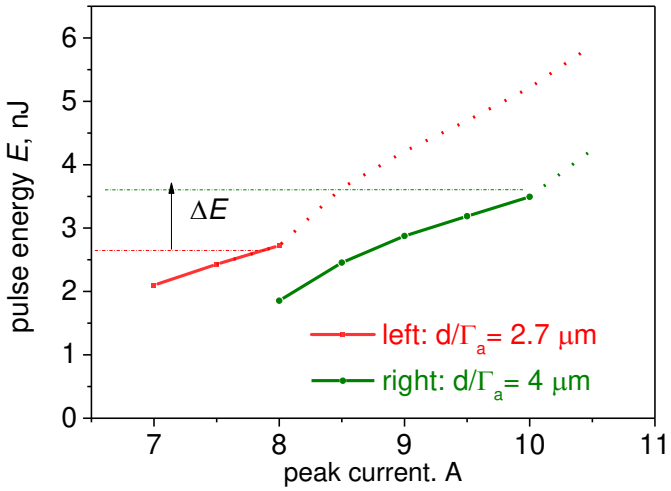

Figure 8. Predicted pulse energy as function of current pulse amplitude for lasers with d/Γ_a of 2.7 μm (as in Figure 4) and 4 μm (as in Figure 7). The solid parts of the curves correspond to afterpulsing-free operation.

Conclusions

We have shown that introducing a SA in the asymmetric waveguide laser cavity can lead to robust generation of high-energy, afterpulse-free picosecond pulses in a broad current range, and that this combination of the large d_a/Γ_a and a saturable absorber leads to laser performance better than what can be achieved by either one of these approaches on its own. A broad temperature operating range is observed.

Acknowledgements

This work was supported by the Academy of Finland (Centre of Excellence in Laser Scanning Research, contract no. 272196, and contract nos. 255359, 283075 and 251571) and the Finnish Funding Agency for Innovation (TEKES). The authors thank A.Gubenko of Innolume GmbH for useful discussions on laser structures.

References

1. P. P. Vasil'ev, "Ultrafast diode lasers: fundamentals and applications", Boston, Artech House, 1995
2. E.U. Rafailov and E.A. Avrutin, in *Semiconductor lasers*, A. Baranov and E. Tournie, Eds (2013), pp. 149-160
3. L. Pancheri; D. Stoppa, "Low-noise single Photon Avalanche Diodes in 0.15 μm CMOS technology", Proc. 2011 European Solid-State Device Research Conference (ESSDERC), Helsinki, 2011, pp. 179 - 182, IEEE, Piscataway, NJ, 2011.
4. B.S. Ryvkin, E.A.Avrutin, J. Kostamovaara 2009 (12), *Journal of Lightwave Technology*, **27**, 2125
5. B.S. Ryvkin, E.A.Avrutin, J. Kostamovaara 2011, *Semicond. Sci. Technol.,* **26** (4), 045010
6. L.W. Hallman, B. Ryvkin, K. Haring, S. Ranta, T. Leinonen and J. Kostamovaara 2010, *Electronics Letters* **46**(1), 65
7. B. Lanz, B.S.Ryvkin, E.A.Avrutin, J. Kostamovaara 2013, *Optics Express*, **21** (24), pp. 29780-29791
8. J. Huikari *et al*. 2015, *IEEE J. Select. Top. Quantum Electron*., **21** (6), paper 1501206
9. B.S. Ryvkin, E.A.Avrutin, J. Kostamovaara 2011 *J. Appl. Phys.* , **110** (12), paper 123101
10. P.W. Juodawlkis *et al*., *IEEE J. Select. Top. Quantum Electron*., 17, (6) , 1698-1714
11. J. Ohya *et al*. 1991, *IEEE J. Quantum Electron*., **27**, 2050-2059
12. E. L. Portnoi *et al*. 1997, *IEEE J. Select. Top. Quantum Electron*., **3,** (2) , 256-260
13. G.B.Venus *et al*., in *Proceedings of 17th IEEE International Semiconductor Laser Conference*, (Monterey, CA, 2000), pp. 145-146
14. M.S. Buyalo *et al*. 2015, *Tech. Phys.Lett*., **41** (10), pp. 984-986
15. S.W.Koch, N. Peyghambarian, H.M. Gibbs 1988, *J.Appl.Phys*., **63** (2), pp. R1-R11
16. D.A.B. Miller *et al*. 1985, *IEEE J. Quantum Electron*., **21** (9), 1462-1476
17. Ryvkin B.S., 1985, *Sov. Phys. Semicond*., **19**, 1-15
18. Ryvkin B.S., Avrutin E.A., Panajotov K. 2009, *Semicond. Sci. Technol.*, **24** (2), p 025001
19. A. Kaltenbach *et al*. 2016, *IEEE Photon.Technol. Lett*., 28 (8), pp. 915-918
20. B.S.Ryvkin, E.A.Avrutin, J. Kostamovaara 2013, *J. Appl. Phys.* , **113** (6), paper 013104
21. D.V. Kuksenkov, R.V. Roussev, S.P. Li, W.A.Wood, and C.M. Lynn 2011, *Proc. SPIE,* 7917 79170B 1-12
22. P. Crump *et al.,* 2013, *IEEE J. Select. Top. Quantum Electron*., **21** (6), paper 1501211

23. P. Crump *et al*., 2014, *Semicond. Sci. Technol.,* **29** (4), 045010

24. Y.Yamagata *et al*. 2015, in: Proceedings of the 2015 High-Power Laser Diodes and Systems Conference, IEEE, 2015, p. 7-8

25. E.A.Avrutin, N.Dogru, B.S. Ryvkin, J.T. Kostamovaara 2016, *IET Optoelectronics*, 10 (2), pp. 57-65

26. R.F. Kazarinov 1973, *Sov. Phys. Semicond*., 7 (4), pp. 525-531

27. L.A. Coldren,S.W.Corzine,M.L.Masanovic, Diode lasers and photonic integrated circuits, Wiley, NY, 2012

28. L. Banyai, S.W.Koch 1986, *Zeitschrift Phys*., **63** (3), 283-291

29. J. Nissinen, J. Kostamovaara, IEEE Sensors Journal, Volume: 16, Issue: 6, Pages: 1628 - 1633, 2016, DOI: 10.1109/JSEN.2015.2503774.

30. L. W. Hallman, J. Huikari, J. Kostamovaara, Proceedings of the IEEE SENSORS conference in 2014, 4p., 2014, 10.1109/ICSENS.2014.6985213

31. J. Kostamovaara, K. Määttä, M. Koskinen, R. Myllylä: Pulsed laser radars with high modulation frequency in industrial applications, Proceedings of the SPIE Conference Laser Radar VII: Advanced Technology for Applications Vol.1633, January 23-24, Los Angeles 1992, pp. 114-127.

Figure captions

Figure 1. The optical output of the laser diode (stripe width 90um, cavity length 1.5mm) as a function of the pulse current. a) saturable absorber length 20um, b) saturable absorber length 100um. Note, that the separate results are shown in a single figure to enable one to compare the results easier.

Figure 2. Optical output spectra of the laser diodes (stripe width 90um, cavity length 1.5mm) with the saturable absorber lengths of 20um and 100um. Drive current pulse amplitude and width ~10A and ~1.5ns, respectively.

Figure 3. Optical output of the laser diode with a cavity length, stripe width and saturable absorber length of 1.5mm, 90um and 20um, respectively, as a function of ambient temperature.

Figure 4. Calculated pulse shapes (filtered) as function of injection current amplitude. For I_{peak}=10 A, parts of an unfiltered profile (pale line) and current pulse are also shown.

Figure 5. Comparison of measured (dots) and simulated (line, solid- afterpulsing-free, dashed-with afterpulses) peak pulse power

Figure 6. Calculated spectra of lasers with 100 and 20 μm long absorbers when pumped by a pulse 10 A in amplitude

Figure 7. Predicted pulse shapes at different current pulse amplitudes for a laser with a larger d/Γ_a value of 4 μm.

Figure 8. Predicted pulse energy as function of current pulse amplitude for lasers with d/Γ_a of 2.7 μm (as in Figure 4) and 4 μm (as in Figure 7). The solid parts of the curves correspond to afterpulsing-free operation.

TABLE I

The values of the main parameters used

Parameter	Value	units
Laser length	1500	µm
confinement factor	0.03	
Stripe width	90	µm
Active region thickness	0.08	µm
HR/AR mirror reflectivity	0.95 / 0.05	
Saturable absorber length	20 or 100	µm
internal (dissipative) loss	0.015	m^{-1}
Injection efficiency (supplied by manufacturer)	0.7	
group refractive index	3.75	
Gain constant g_0 in (1)	27	m^{-1}
Gain spectrum width $\Delta\omega$ at transparency	$3\cdot10^{13}$	s^{-1}
Gain peak shift with carrier density	$1.6\cdot10^{-11}$	$s^{-1}m^3$
Gain spectrum broadening with carrier density	$3.2\cdot10^{-11}$	$s^{-1}m^3$
gain compression coefficient	$3\cdot10^{-23}$	m^3
Unsaturated absorption	100	m^{-1}
Absorption cross-section σ in (2)	$5.4\cdot10^{-19}$	m^2
SA compression coefficient	$3\cdot10^{-23}$	m^3
bimolecular recombination factor	$1.5\cdot10^{-16}$	m^3/s
Auger recombination coefficient	$2\cdot10^{-41}$	m^6/s
Absorber recovery time	5	ns
Henry factor, gain section	5	
Henry factor, absorber section	1	